Pergamon

Chaos, Solitons & Fractals Vol. 5, No. 1, pp. 15–23, 1995
Elsevier Science Ltd
Printed in Great Britain.
0960-0779/95$9.50 + .00

0960-0779(94)00207-X

Dimerized Island Chains in Tokamaks

GISELE A. ODA and IBERÊ L. CALDAS

Institute of Physics, University of São Paulo, C.P. 20516, 01498-970-São Paulo, SP-Brasil

(*Received* 19 *July* 1994)

Abstract—Magnetic surfaces are studied on MHD equilibrium plasmas with non-monotonic safety factor radial profiles, confined on large aspect-ratio tokamaks. Perturbing helical windings lead to twin Poincaré–Bhirkhoff chains and reconnection phenomenon, giving rise to dimerized island chains. Evolution of radial rotation number profiles, together with the radial progression of equilibrium points clarify the reconnection process. Toroidal perturbation leads to reconnection for values of the parameter I_h much lower than those in the integrable case. Then, for higher I_h, we have overlap of secondary islands and the onset of chaotic regions from the edge region to the center.

Given a magnetic field **B(r)** which confines a plasma, the magnetic field line trajectories are determined by integrating the differential equation [1]:

$$\mathbf{B} \times d\mathbf{l} = 0. \tag{1}$$

In the case of a plasma confined in a tokamak in static MHD equilibrium, this equation can be analytically integrated. Thus, the field lines lie on KAM toroidal magnetic surfaces and the trajectories are either periodic or quasi-periodic [1]. However, the existence of natural or external perturbations create resonances which modify the trajectory topology and give rise to magnetic islands and chaotic trajectories [2].

We consider in this paper large aspect-ratio tokamaks ($R \gg a$, where R is the major radius of the toroidal camera and a is the plasma column radius, see Fig. 1), leading to

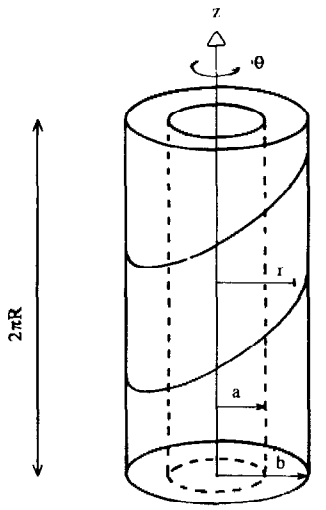

Fig. 1. Scheme of a tokamak in the cylindrical approximation, with perturbing helical windings.

cylindrical approximation. In this case, the unperturbed field is a superposition of a uniform field B_z^0, created by external coils, and a field B_Θ^0, created by a central hole plasma current density [Fig. 2(a)]:

$$\mathbf{j} = j_0\left(1 + \beta\frac{r^2}{a^2}\right)\left(1 - \frac{r^2}{a^2}\right)^\mu \mathbf{e}_z. \tag{2}$$

(The cylindrical coordinates are indicated in Fig. 1.)

For the considered plasma current profile, the rotation number ρ, defined as [3]:

$$\rho(r_0, \Theta_0) = \lim_{N\to\infty} \frac{1}{2\pi N} \sum_{n=1}^{N} (\Theta_i - \Theta_{i-1}) \tag{3}$$

or the safety factor, $q = \rho^{-1}$, more used in the fusion plasma literature, is not monotonic [Fig. 2(b)]. These profiles have been observed in tokamaks, at the initial stages of electrical discharges [4–6], and could trigger the double tearing mode instability [7]. They can also be found after the plasma current reaches the maximum value [8] or as the confined plasma is submitted to a high power neutral beam injection [9].

In this work, we choose $q(a) = 3.9$, $q(0) = 3.2$, $\beta = 2$, $\mu = 1$, $R = 0.30m$, $a = 0.08m$, corresponding to the parameters of the tokamak TBR-1 [10].

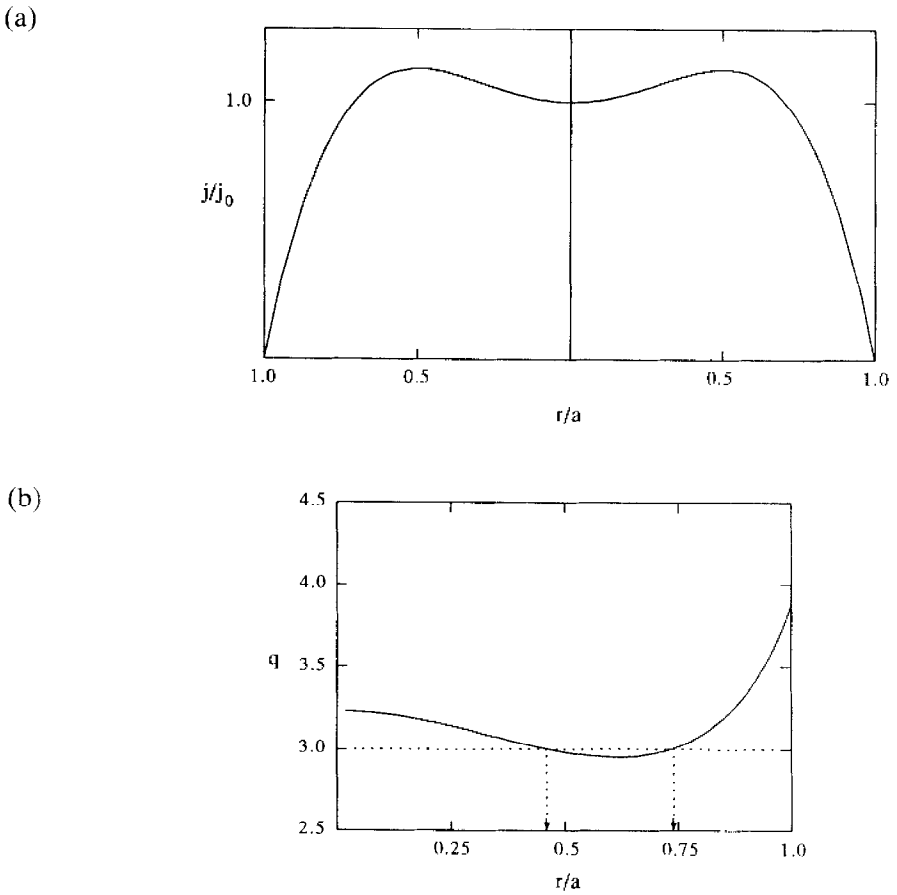

Fig. 2. (a) Central hole plasma current density radial profile; (b) safety factor radial profile. Radial positions of $q = 3/1$ surfaces are indicated.

The unperturbed KAM surfaces constitute a family of nested cylindrical surfaces. The rational surfaces have $q = m/n$ (m, n integers). For a given q value, there are two rational surfaces with different radii in the internal region.

Perturbations are considered due to m pairs of equidistant helical windings [11] conductors of radius b. Adjacent conductors have currents I_h with opposite directions (Fig. 1). The magnetic field due to these helical currents is [10]:

$$\mathbf{B}_1 = \nabla\Phi$$

$$\Phi \approx -\frac{\mu_0 I_h}{\pi}\left(\frac{r}{b}\right)^m \sin u, \tag{4}$$

where $u = m\Theta - (n/R)z$. Constant coordinates u and r characterize a helix.

Since the perturbation field is much weaker than the equilibrium field,

$$\mathbf{B}_1/\mathbf{B}_0 \ll 1, \tag{5}$$

we consider the perturbed field as a linear superposition:

$$\mathbf{B} \simeq \mathbf{B}_0 + \mathbf{B}_1. \tag{6}$$

This approximation is not valid for marginally stable states when the plasma response should not be neglected.

Introduction of canonical variables leads to the equations of field line motion in the form of Hamilton equations [12]:

$$\frac{\partial H}{\partial u} = \frac{\mathrm{d}\rho}{\mathrm{d}t} \qquad \frac{\partial H}{\partial \rho} = -\frac{\mathrm{d}u}{\mathrm{d}t} \tag{7}$$

(where $\rho = r^2/2$) with the Hamiltonian [13]:

$$H = \left(\frac{nB_z^0}{R} - \frac{m\mu_0 I_p}{\pi a^2}\right)\rho - \frac{m\mu_0 I_p}{2\pi a^4}\rho^2 + \frac{8m\mu_0 I_p}{9\pi a^6}\rho^3 + \frac{\mu_0 I_h m}{\pi}\left(\frac{r}{b}\right)^m \cos u. \tag{8}$$

Analytical Poincaré maps are obtained considering magnetic surfaces of constant Hamiltonian.

A resonant effect at the surfaces with $q = m/n$, due to the considered perturbative field, gives rise to chains of m islands. In this work, we consider $m = 3$, $n = 1$. Figure 3(a) shows twin Poincaré–Birkhoff chains [3] with 3 islands at the two surfaces with $q = 3/1$. Increasing values of I_h lead to the enlargement of the islands in both chains [12], until they join together. From this critical value of the parameter above, starts the reconnection of field lines [14], which gives rise to two dimerized island chains [3], as shown in Fig. 3(b). After the bifurcation takes place [Fig. 3(c)], only one internal dimerized chain is left.

Equilibrium points are located where $\nabla H = 0$. The Θ-positions are, thus, $n\pi/3$ ($n = 0$, 1, 2, 3, 4, 5) and will be considered the principal Θ-directions for the following analysis. The radial positions depend on the angle and parameter I_h value.

Fixing a Θ-direction on a map at parameter value I_h, a radial ρ profile can be set by numerical integration. As we consider Θ-directions passing through the equilibrium points, a plateau of constant $\rho = 1/3$ corresponds to the extension of the islands and a point of $\rho = 1/3$ to the hyperbolic point. The evolution of these ρ-profiles, as the control parameter takes increasing values, is similar to that reported in refs [3, 13]. ρ-profiles at $\Theta = 0$ and $\Theta = \pi/3$ present distinct evolution after the plateau reaches the hyperbolic point, or better, after the reconnection takes place: the former shows diminution of the plateau, until the bifurcation value of I_h, after which all the curve lies below the $\rho = 1/3$ value [Fig. 4(a)].

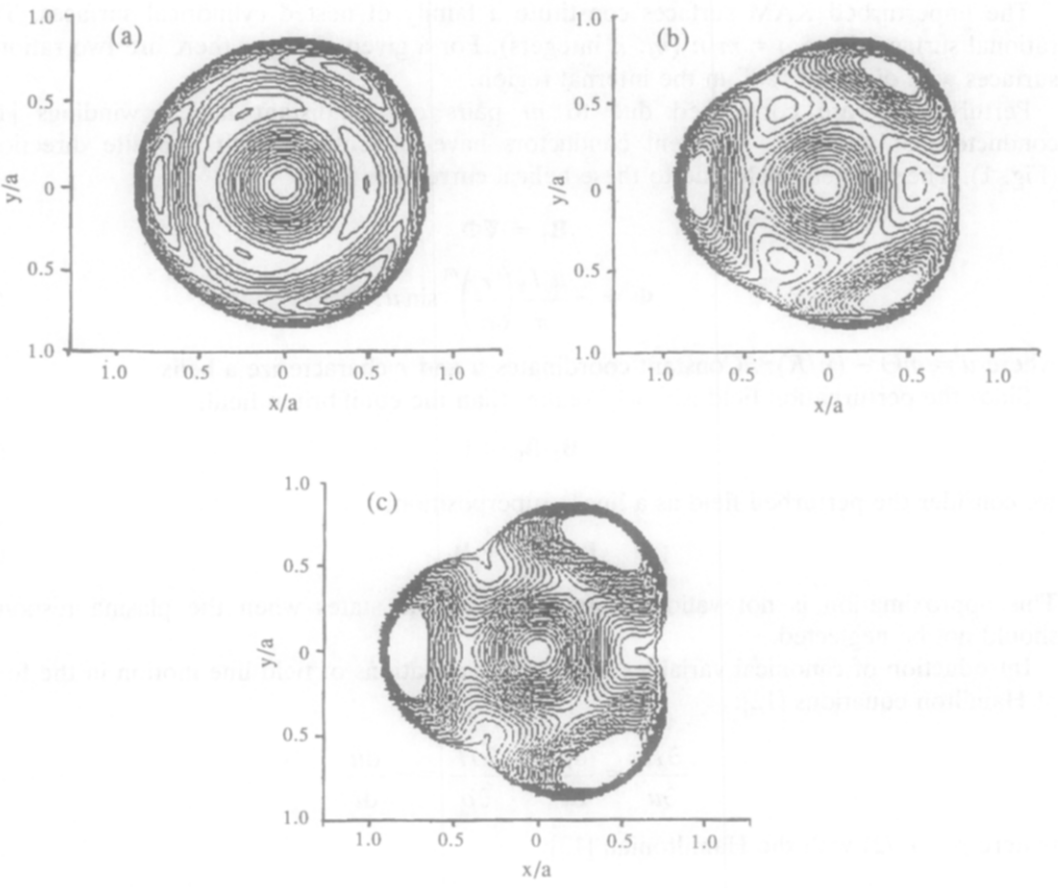

Fig. 3. Analytical Poincaré Maps of the equilibrium plasma perturbed by helical current. (a) $I_h = 25$ A; (b) $I_h = 100$ A; (c) $I_h = 154$ A.

The latter shows constant enlargement of the plateau as the island at this angle, corresponding to the internal dimerized chain, 'survives' [Fig. 4(b)].

Fixing a principle Θ-direction, radial progression of equilibrium points can also be shown on a graph. Figure 5(a) shows the relative distances of pairs of equilibrium points at $\Theta = 0$: as the parameter I_h is increased, the equilibrium points of the two chains approximate from each other until they are collapsed at the bifurcation value of the parameter ($I_h = 154$ A). At higher values of I_h, they leave the real plane. On the other hand, Fig. 5(b) shows the equilibrium points at $\Theta = \pi/3$, moving away from each other. Note, however, that a crucial transformation has occurred to the considered pairs of equilibrium points during their radial progressions: before the reconnection, one elliptic and one hyperbolic point of distinct Poincaré–Birkhoff chains form a pair; after the reconnection, one elliptic and one hyperbolic point of the same dimerized chain form a pair.

Islands in twin chains are $\pi/3$ out of phase, because the Jacobian eigenvalues of this system, corresponding to equilibrium points standing at the same angle Θ, always assume opposite signs. There is no parameter change modifying this fact, or better, leading to aligned islands, in our system [13].

A toroidal perturbation is considered upon the system, which loses integrability and becomes almost integrable [11].

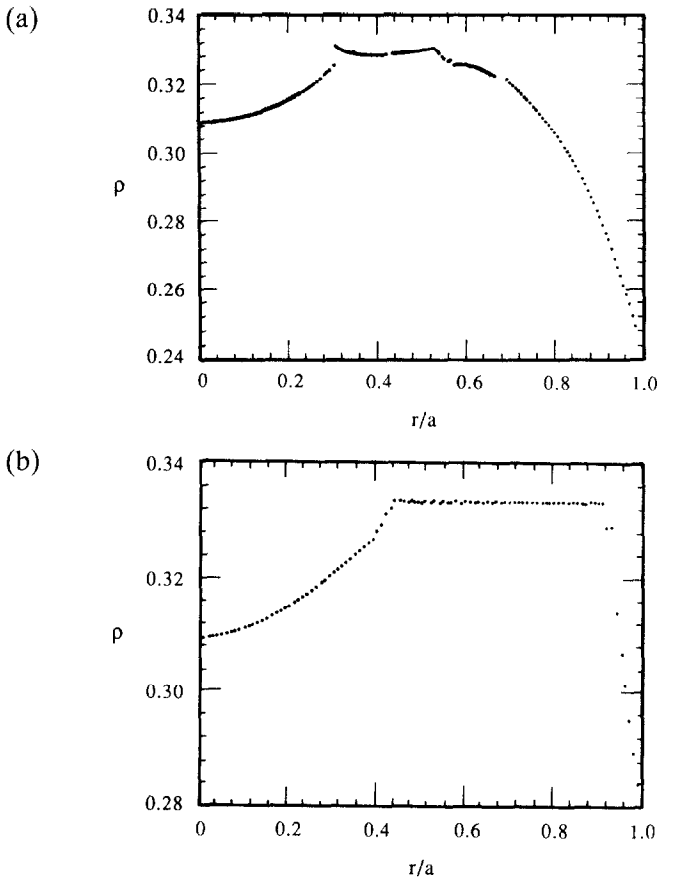

Fig. 4. Radial ρ-profiles for $I_h = 154$ A. (a) $\Theta = 0$; (b) $\Theta = \pi/3$.

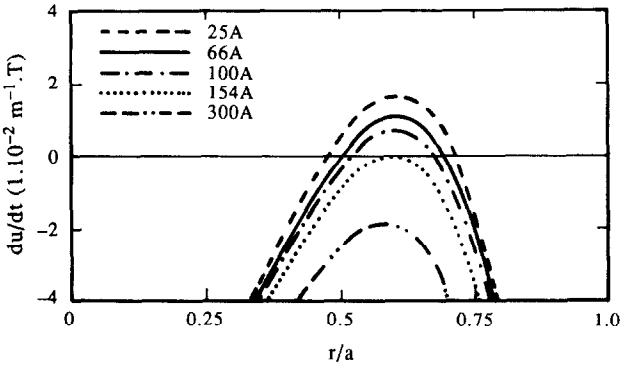

Fig. 5. Radial approaching of equilibrium points as I_h takes increasing values at $\Theta = 0, 2\pi/3, 4\pi/3$.

The Poincaré maps, in this case, are obtained by numerical integration of (1) in the form:

$$\frac{dr}{B_r} = \frac{r d\Theta}{B_\Theta} = \frac{dz}{B_z}. \tag{9}$$

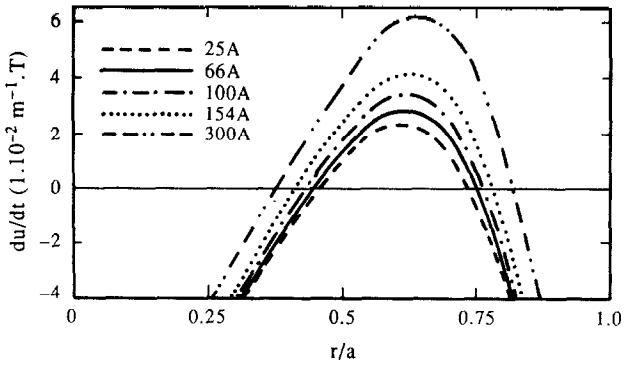

Fig. 6. Radial distancing of equilibrium points as I_h takes increasing values at $\Theta = \pi/3, \pi, 5\pi/3$.

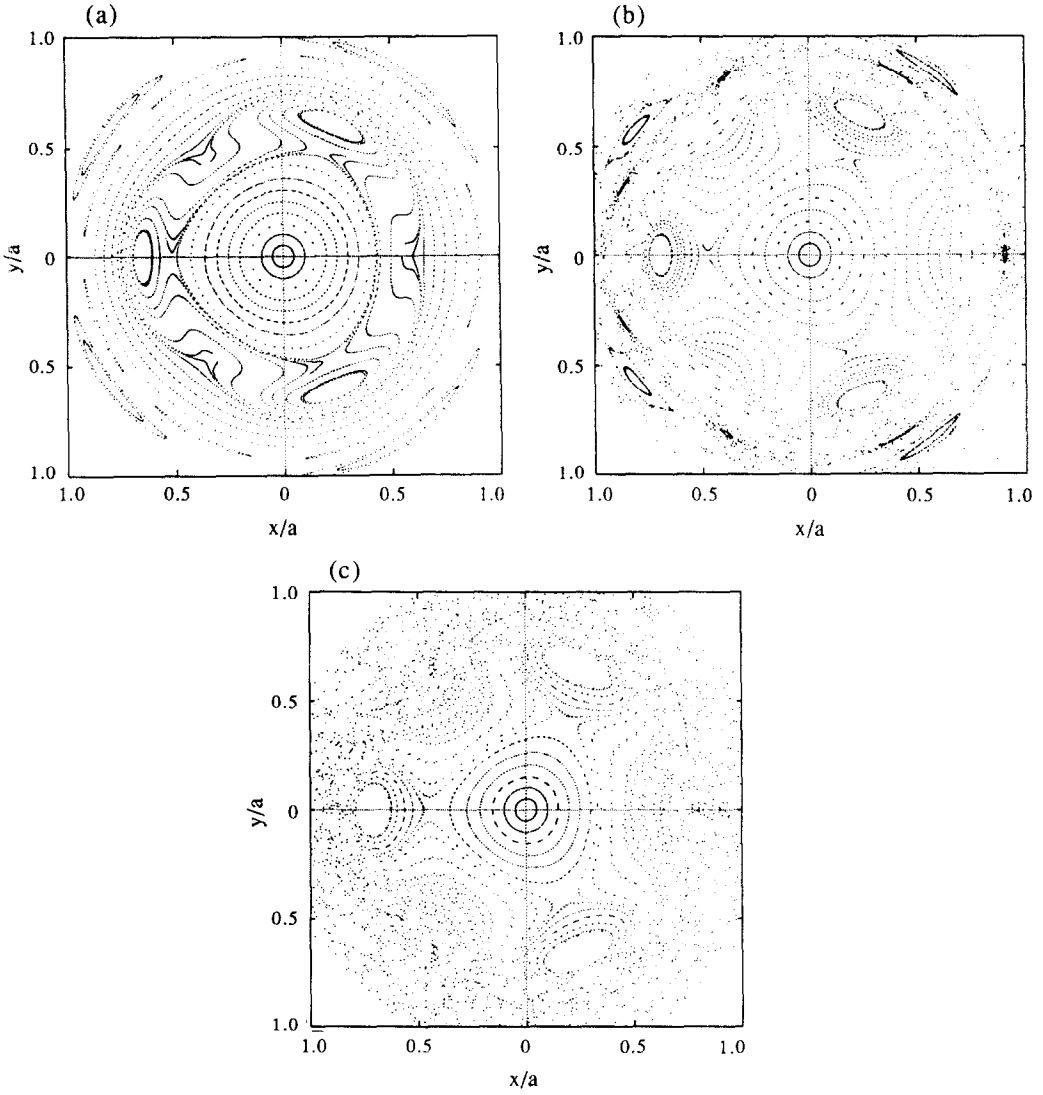

Fig. 7. Numerical Poincaré maps of the system after toroidal correction. (a) $I_h = 25$ A; (b) $I_h = 100$ A; (c) $I_h = 154$ A.

The toroidal effect is introduced by modifying the uniform field B_z^0, as we consider the field generating solenoid wound along a torus. The components B_r and B_Θ are the equilibrium ones, since their amplitudes are much weaker than B_z, affecting less the perturbed map. So, we have:

$$B_z = \frac{B_z^0}{1 + \frac{r}{R}\cos\Theta} + \frac{\partial\Phi}{\partial z}$$

$$B_r = \frac{\partial\Phi}{\partial r}$$

$$B_\Theta = B_\Theta^0 + \frac{\partial\Phi}{\partial\Theta} \tag{10}$$

where Φ is defined in (4) and B_Θ^0 is obtained by applying Ampère's law to the current density (2).

The whole map does not present axial symmetry, as shown in Fig. 7. The toroidal effect approximates the island chains, leading to a reconnection phenomenon early at low values of I_h, when the islands are still not large. Thus, in the numerical Poincaré map shown in Fig. 7(a), we already have, for $I_h = 25$ A, only the internal dimerized chain, corresponding to a step after bifurcation of the equilibrium points of the external chain. Note that, for the same I_h, corresponds two Poincaré–Birkhoff chains at the integrable case.

We find also secondary islands near the edge ($r/a \approx 1$). They come from the resonant effect at all the surfaces with rational $q = m/n$ spanned in the interval of Fig. 2(b). In the scale of the figure, we see mainly those islands standing at the edge ($r/a \approx 1$), because the perturbative effect is stronger for large r. Also in the considered region and scale we can detect only the secondary islands corresponding to $q = 4/1$ and $q = 7/2$, since the width of the islands decrease rapidly for growing n [3]. Thus, gradual amplification of the scale of the figure may detect more and more infinitely small islands, showing a fractal structure [Fig. 9(a)]. Corresponding radial ρ-profiles have infinite plateaux for the islands, showing a typical 'devil's staircase' structure [Fig. 9(b)].

Increasing values of the parameter I_h cause the superposition and destruction of these islands, giving rise to chaotic regions [15], as shown in Fig. 7(b). In Fig. 9(b) we can already see a first chaotic region rising at $r/a \approx 0.95$, where the ρ-profile does not converge. Thus, the chaotic lines rise initially in the edge region and expand to the center, as I_h is increased. This fact can be seen in Fig. 8, where a distinct limit of the regular and chaotic regions are shown for the radial ρ-profiles of the perturbed case. For greater values of I_h [Fig. 7(c)], a chaotic region can also be seen (in the scale of the figures presented here), in the vicinity of the internal separatrices at $\Theta = \pi, \approx\pi/3, \approx 4\pi/3$.

The rise and evolution of the chaotic region, described here, correspond to the effect of the toroidal perturbation given as (9), upon the system characterized by the parameters $\mu = 1$ and $\beta = 2$. Other expressions for considering the toroidal effect on the system may give slightly different evolution picture, as I_h takes increasing values. In [16], the first chaotic lines rise from the splitting of the low energy separatrices and then, for higher control parameter, also from the high energy separatrices. The non-integrable map, corresponding to the bifurcation parameter value of the integrable case, showed that even after the hyperbolic orbit had vanished from the real plane, the region remained as concentrating the chaotic orbits [16]. In our system, however, the external separatrices (corresponding to the low energy separatrices for [16]), vanish early for low values of I_h,

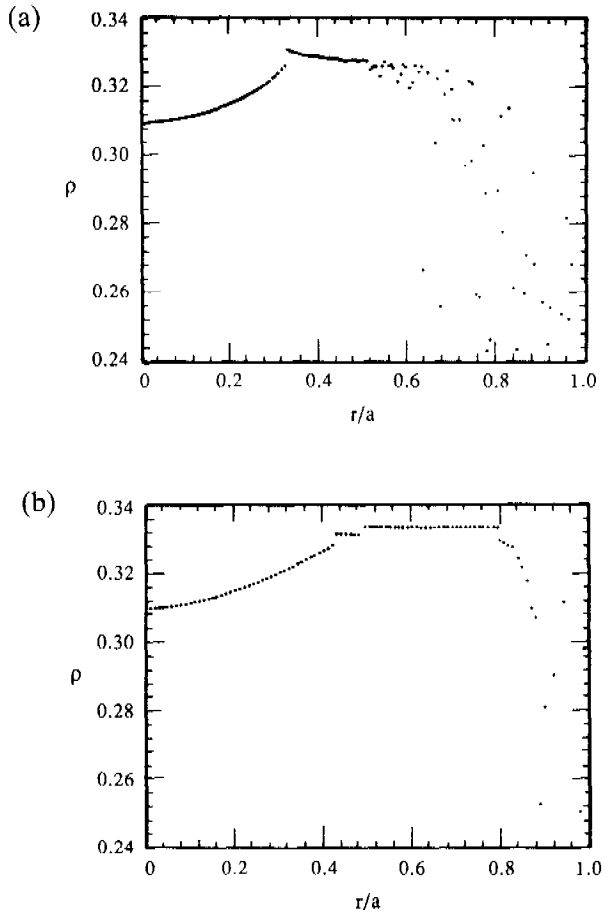

Fig. 8. Radial ρ-profiles of the system after toroidal correction, for $I_h = 154$ A. (a) $\Theta = 0$; (b) $\Theta = \pi/3$.

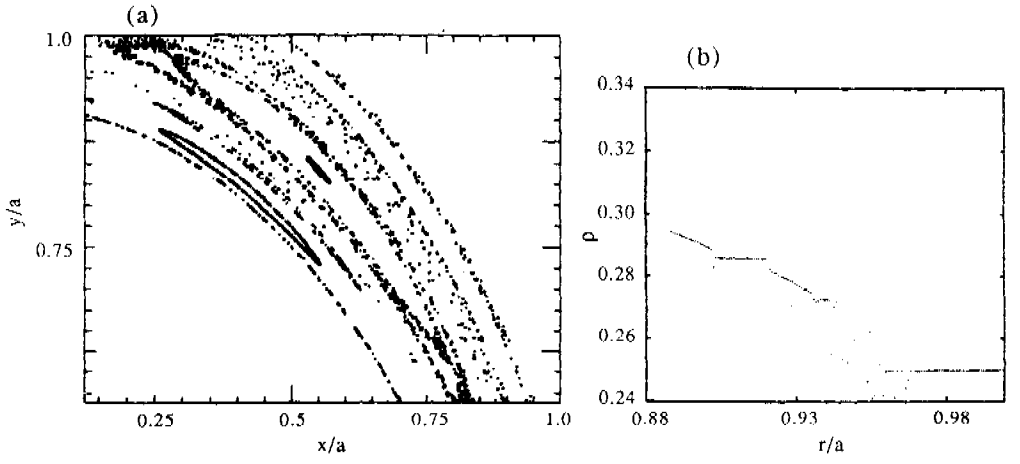

Fig. 9. (a) Magnification of a numerical Poincaré map of the system with toroidal correction, for $I_h = 55$ A, showing infinite secondary islands; (b) corresponding radial ρ-profiles showing 'devil's staircase' structure ($\Theta \approx \pi/4$).

and the chaotic lines rise first in the overlap region of secondary islands. Then, also for higher values of I_h, they rise from the destruction of the internal separatrices.

In both pictures, the perturbation effect has non-uniform strength over the coordinate space under consideration and is stronger for higher values of the control parameter. Also the choice of other parameters μ and β may change the evolution picture, since these parameters are responsible for the curvature of the q-radial profile and, consequently, for the distance of the two chains from each other and from the edge. A combination of these factors give rise to the different evolution pictures of chaotic lines for increasing parameters.

Reconnection has been studied in many physical systems [14], and here we presented the phenomenon in the description of the magnetic surfaces of non-monotonic q-radial profile plasmas.

Acknowledgements—The authors thank the discussions with Drs A. M. Ozório de Almeida (IFGW-UNICAMP), R. E. Carvalho (UNESP), Drs P. M. Morrison and D. Del Castillo-Negrette (IFS-University of Texas). This work was partially supported by CNPq.

REFERENCES

1. A. I. Morozov and L. S. Solov'ev, The structure of magnetic fields, *Reviews of Plasma Physics* **2**, 1 (1966).
2. D. C. Robinson, Ten years of results from the TOSCA device, *Nuclear Fusion* **25**, 1101–1108 (1985).
3. J. P. Van der Weele, T. P. Valkering, H. W. Capel and T. Post, The birth of twin Poincaré–Birkhoff chains, *Physica A* **153**, 283–294 (1988).
4. D. Dimock and H. Johnson, The ontogeny of a tokamak discharge, *Nuclear Fusion* **13**, 271–280 (1973).
5. K. Makishima, T. Tominaga, H. Toyuama and S. Yoshikawa, Simultaneous measurements of the plasma current profile and instabilities in a tokamak, *Physical Review Letters* **36**, 142–145 (1976).
6. D. Del Castillo-Negrette and P. J. Morrison, *Bulletin of the American Physical Society* **37**, 1542 (1992).
7. W. Kerner and H. Tasso, Stability of multihelical tearing modes in shaped tokamaks, *Physical Review letters* **49**, 654–657 (1982).
8. N. R. Sauthoff, S. von Goeler and W. Stodiek, Report PPPL-1379, Princeton (1977).
9. Recent DIII-D Results, *Proc. of the XIV International Conference on Plasma Physics and Controlled Fusion Research* (Wurzburg, 1992), paper IAEA-CN-56/A-1-2 (1993).
10. A. S. Fernandes, M. V. Heller and I. L. Caldas, The destruction of magnetic surfaces by resonant helical fields, *Plasma Physics and Controlled Fusion* **30**, 1203–1211 (1988).
11. F. Karger, H. Wobig and S. Corti, Influence of resonant helical fields on tokamak discharges, In *Proc. of the 6th International Conference on Plasma Physics and Controlled Nuclear Fusion Research* (Tokyo, 1973), IAEA 1. 207 (1974).
12. M. C. R. Andrade, Formulação Hamiltoniana para superfícies magnéticas, M.Sc. dissertation, IFUSP (1990).
13. G. A. Oda, Reconexão de linhas de campo em tokamaks, M.Sc dissertation, IFUSP (1993).
14. J. E. Howard and S. M. Hohs, Stochasticity and reconnection in Hamiltonian systems, *Physical Review A* **29**, 418–421 (1984).
15. B. V. Chirikov. A universal instability of many-dimensioned oscillator systems, *Physics Reports* **52**, 263 (1979).
16. R. E. Carvalho and A. M. Ozorio de Almeida, Integrable approximation to the overlap of resonances, *Physics Letters A* **162**, 457–463 (1992).